Xenon 147-nm resonance f value and trapped decay rates

H. M. Anderson,[1] S. D. Bergeson,[1] D. A. Doughty,[2] and J. E. Lawler[1]
[1]*Department of Physics, University of Wisconsin—Madison, Madison, Wisconsin 53706*
[2]*Corporate Research and Development Center, General Electric Company, P.O. Box 8, Schenectady, New York 12301*
(Received 10 May 1994)

The absorption oscillator strength of the xenon 147-nm resonance transition is measured to be 0.264 ± 0.016. This value is from direct absorption measurements with equivalent widths from ≈ 1 to ≈ 10 cm^{-1}. This f-value measurement is compared to others in the literature and is used in Monte Carlo simulations of trapped decay rates. The simulations include an angle-dependent partial frequency redistribution. The simulation results are compared to trapped decay rates in the literature.

PACS number(s): 32.70.Cs, 32.70.Jz

I. INTRODUCTION

Atomic xenon has been identified as a possible candidate for replacing mercury in fluorescent lighting discharges [1]. Mercury is toxic and thus represents an environmental hazard; a nontoxic replacement is desired. To this end, a highly quantitative understanding of resonance radiation trapping for the xenon 147-nm transition is needed. Recent work on this radiation transport problem [2] has not resolved the discordance between experimental results and simulations. Trapped decay rates measured by Vermeersch *et al.* [2] were typically 10–30 % larger than trapped decay rates from Monte Carlo simulations. We report a precise measurement of the oscillator strength (f value) for the 147-nm resonance transition. We use this refined f value in a radiation transport simulation and compare to measurements of trapped decay rates for atomic xenon by Vermeersch *et al.* [2]. Our refined f value eliminates the discordance in the trapped decay rates.

Many measurements of the xenon 147-nm f value have been made using a variety of techniques. We use the absorption method, which is the simplest, most direct method for finding oscillator strengths. Two previous determinations also used this approach [3,4]. Wilkinson's measurements were flawed by large equivalent widths and high pressures [3]. The line profile and model he used to analyze his experiment were inappropriate and thus his result, by itself, cannot be trusted [3]. The result of Chashchina and Shreider is of limited accuracy [4]. Since these early measurements, the theory of spectral line profiles has improved. Resonance collisional broadening in the impact approximation is now well understood and a more precise determination of the xenon 147-nm f value using the absorption method is appropriate.

The next section describes the curve of growth used to analyze our absorption data. Section III describes our absorption experiment. Section IV presents the results of the absorption experiment, and a comparison to earlier work on the xenon 147-nm f value. Section V describes our Monte Carlo simulations and compares the results of the simulations to experimental trapped decay rates by Vermeersch *et al.* [2]. Finally, Sec. VI is a summary.

II. CURVE OF GROWTH THEORY FOR XENON 147-nm LINE

The equivalent width in units of cm^{-1} from an absorption measurement is

$$W=\int (1.0-T_a)\frac{d\nu}{c}\ , \tag{1}$$

where T_a is the transmittance of the absorbing sample, ν is the frequency, and c is the speed of light. The integral extends across the entire line profile. The function relating the equivalent width to the column density is the curve of growth. An absorption measurement on an optically thin gas yields an equivalent width that is equal to the product of the absorption oscillator strength, column density, and πr_e where r_e is the classical radius of the electron. As the opacity at line center increases, the linear relation between equivalent width and column density breaks down. A more complex curve of growth is required to relate these quantities in general. For resonance transitions in gases, the linear part of the curve of growth is realized only for very small column densities, meaning very low pressures or very short path lengths. In our experiment, the opacity at line center is extremely high. Absorption at line center is complete and the equivalent width is dominated by absorption in the wings of the line profile. In this limit, an analytic expression for the curve of growth is found. This analytic expression neglects the effects of isotopic and hyperfine structure and Doppler broadening, and it includes the effects of radiative broadening and resonance collisional broadening.

At small equivalent widths the hyperfine and isotopic structures of the line profile are important for computing a reliable curve of growth. The total width of the hyperfine structure of the resonance $5p^5 6s\ ^3P_1^o$ level ($6s[3/2]1$ in Racah notation) of the only stable odd isotopes ^{129}Xe and ^{131}Xe are 0.05 and 0.04 cm^{-1}, respectively [5]. To our knowledge, there is no published information on the isotope shifts for the 147-nm transition. However, parameterized isotope shift studies of different levels in xenon have been made [6]. The field shifts and specific mass shifts of the resonance $5p^5 6s\ ^3P_1^o$ level ($6s[3/2]1$) with respect to a $5p^5 7p$ level ($7p[1/2]1$) are

known. Although the field shifts and specific mass shifts (or residual isotope shifts) of the ground $5p^6\,{}^1S_0$ level are not known, the field shifts are likely to be small because the p electrons do not penetrate the nucleus. We combine the residual isotope shifts of the resonance level with the reduced mass shifts of the 147-nm transition to estimate the isotopic structure of the transition. This approach gives an isotope shift of 0.026 cm^{-1} between the ^{136}Xe and ^{128}Xe components of the 147-nm transition. A conservative estimate of the extent of the total hyperfine and isotopic structure for the 147-nm transition is 0.1 cm^{-1}. We establish by direct measurement, discussed in the next section, that this structure is significantly less than 0.9 cm^{-1} in extent. The curve of growth for equivalent widths larger than ≈ 1 cm^{-1} is not sensitive to this structure. With detailed knowledge of the hyperfine and isotopic structure, a curve of growth can be computed and used to extract f values from absorption measurements with small equivalent widths. In the absence of this information, ≈ 1 cm^{-1} poses a conservative lower limit on the equivalent width in our experiment. The Doppler width of the xenon resonance line is 0.07 cm^{-1} at room temperature, it may also be neglected in computing the curve of growth for equivalent widths greater than 1 cm^{-1}.

Radiative broadening contributes a Lorentzian line profile with a well-known width. The theory of resonance collisional broadening in the impact approximation is much better developed now than it was when earlier absorption experiments were performed. Corney reviews theoretical and experimental work on resonance collisional broadening [7]. He also gives a simple expression for the contribution to the width of the Lorentzian line profile from resonance collisions in the impact approximation. The impact approximation assumes discrete (well separated in time) collisions with a single perturber, and thus is limited to xenon gas pressures below several hundred Torr. This is not a serious limit since our experiment is at pressures of 1.0 Torr and below. The impact approximation is also limited to regions within several cm^{-1} of line center because a quasistatic approximation is appropriate for the more extreme wings of the line profile. Fortunately, the theory of resonance collisional broadening in the quasistatic approximation also leads to a Lorentzian line profile with nearly the same expression for the collisional contribution to the width as in the impact approximation. We shall use a Lorentzian profile with a width determined by the sum of resonance collisional broadening in the impact approximation and radiative broadening to calculate a curve of growth for equivalent widths smaller than 10 cm^{-1}.

At very high equivalent widths, absorption features often become asymmetric. For example, the "blue" portion of the xenon resonance line profile is suppressed and the "red" portion is enhanced. An asymmetric absorption profile at very high equivalent widths can be caused by several effects including: (1) the thermal energy k_BT limiting the approach of the resonance and ground-state atoms on a repulsive potential curve, (2) a breakdown of the simple inverse cube expression for the resonance potential curve, and (3) a breakdown of the single perturber approximation. Clearly with $k_BT/(hc) \approx 200$ cm^{-1} at room temperature a simple theory of the line profile, which uses a Boltzmann factor of 1, will only be useful in generating a curve of growth for equivalent widths $\ll 200$ cm^{-1}. Here k_B is Boltzmann's constant, T is the absolute temperature, and h is Planck's constant.

The expression we use to analyze data from our experiment is

$$W^2 = \left[1 + \frac{\lambda^3 N g_u}{65.71 g_l}\right] \frac{8\pi^2 N t f_{lu}^2 g_l r_e^2}{\lambda^2 g_u}, \tag{2}$$

where λ is the wavelength, N is the density of absorbing atoms, t is the length of the absorption cell, g_u (g_l) is the upper (lower) level degeneracy, and f_{lu} is the absorption oscillator strength. In summary, this expression is derived using a pure Lorentzian line profile with a width determined by the sum of the resonance collisional broadening in the impact approximation and radiative broadening. In the parentheses of Eq. (2), radiative broadening is represented by the first term, and resonance collisional broadening in the impact approximation [7] is represented by the second term. Equation (2) is derived assuming a very high opacity at line center. It is believed to be accurate for the 147-nm line with 1 $cm^{-1} \leq W \leq 10$ cm^{-1}, and $N \leq 3 \times 10^{18}$ cm^{-3}.

III. EXPERIMENT

A classic absorption experiment, such as ours, requires a continuum source, an absorption cell, and a spectrometer. The apparatus should be designed to facilitate convenient, very accurate measurements of the equivalent width, the gas density, and the length of the absorption cell.

An argon mini-arc from the National Institute of Standards and Technology is used as a continuum source [8]. This source was developed as a secondary radiometric standard in the vacuum ultraviolet. It is simple, reliable, and it provides a bright continuum at 147 nm.

The absorption cell must be designed to produce equivalent widths between ≈ 1 cm^{-1} and ≈ 10 cm^{-1}. It must also be designed to allow for very accurate measurements of the gas density N and cell length t. (We note that the difficulty of measuring low pressures, $\ll 1$ mTorr, to high accuracy causes a measurement of f_{lu} on the linear part of the curve of growth to be much more challenging.) Even for measurements of W in our chosen range, it is desirable to make t small so that N corresponds to pressures of 1 Torr to a fraction of a Torr. This pressure range can be measured very accurately with modest effort.

Our absorption cell has o-ring sealed LiF windows. The separation of these windows is set by an accurately machined stainless steel spacer that determines the length of the absorption cell. Two spacers of length 0.2627 and 0.9665 cm are used. The cell is evacuated, outgassed, and backfilled with xenon. A capacitive manometer is used to measure the xenon pressure to ± 1 mTorr while monitoring the cell temperature to ± 0.5 K. The absolute calibration of the MKS Inc. baratron is checked against an oil

filled manometer and is found to be accurate to within 1%.

A 3-m focal length McPherson vacuum Czerny-Turner spectrometer with a 1200 groove/mm grating is used in first order for absorption measurements. Typical entrance and exit slit widths are 0.025 and 0.040 mm. A Hamamatsu R1220 photomultiplier with a CsTe cathode and MgF_2 window is used. This detection system is found to be linear over the range of signal levels measured in this experiment. The 3-m focal length spectrometer with a 300 groove/mm echelle grating is used in 40th order with 0.05-mm slits to observe the xenon 147 line in emission from a low pressure glow discharge. This observation provides the experimental upper limit of 0.9 cm^{-1} for the width of hyperfine and isotopic structure.

IV. RESULTS ON THE f VALUE FOR THE XENON 147-nm LINE

Figure 1 shows the results of the xenon 147-nm f value for different xenon densities, absorption cell lengths, and equivalent widths. Each point on the figure is an average of two separate measurements. The error bars represent the reproducibility of the measurements. The f value, as derived using Eq. (2), is observed to be independent of equivalent width. A weighted linear least-squares fit of the f value as a function of density is performed and zero slope is obtained. Specifically, the data of Fig. 1 is fitted to $f_{lu}=AN+B$, yielding $A=(0.0000\pm0.0010)\times10^{-15}$ cm^3. A weighted linear least-squares fit of the f value as a function of equivalent width is also performed and zero slope is obtained. Here the data of Fig. 1 is fitted to $f_{lu}=A'W+B'$, yielding $A'=(0.0002\pm0.0020)$ cm. This demonstrates the validity of the line shape theory used to analyze data from the absorption experiment. Combining all the data for 0.83 $cm^{-1}\le W\le10.32$ cm^{-1}, and $N\le3.34\times10^{16}$ cm^{-3} gives a final oscillator strength for the xenon 147-nm transition of $f_{lu}=0.264(16)$, where the number in parentheses is the uncertainty in the last digits. This 6% uncertainty represents 2σ statistical uncertainty and an estimate of systematic errors from a weighted analysis of data in Fig. 1.

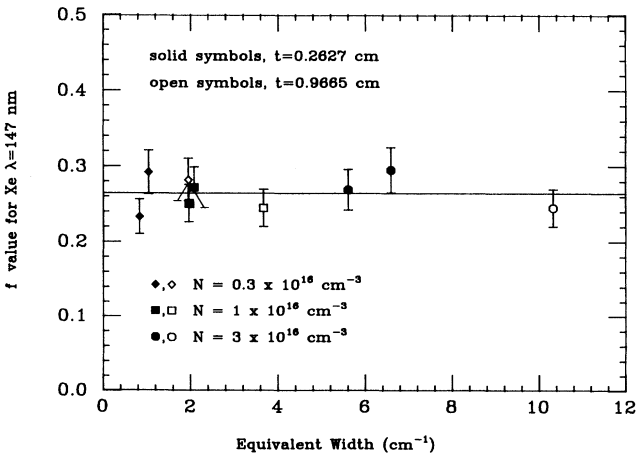

FIG. 1. Xenon 147-nm f value as a function of equivalent width, for different xenon densities and absorption cell thicknesses t.

Table I compares our f value to many other experimental and theoretical values from the literature. The source, f value, and experimental or theoretical method are shown. Chashchina and Shreider [4] and Wilkinson [3] both used the absorption method, as we do, with some variations. Chashchina and Shreider [4] use a line absorption method, where the source of 147-nm light to be absorbed is emitted from a xenon-helium discharge. This kind of absorption measurement requires detailed knowledge of the line shape from the emission source, which was approximated as a Gaussian in their experiment. As a result, their result is of limited accuracy (18%). This method should be contrasted with ours, where the spectral radiance of the continuum source is constant across the xenon 147-nm absorption profile, allowing a much simpler analysis of the experimental data. The experiment of Wilkinson [3] is analogous to ours, but he worked at much higher xenon pressure than those included in this experiment. At higher pressures and large equivalent widths, the curve of growth becomes more complicated due to pressure shifts, satellite formation, quasistatic interactions between xenon atoms, a breakdown of the single perturber approximation, and other effects. Curiously, even though the curve of growth used by Wilkinson is inappropriate for his experimental conditions, his result agrees with ours. However, recent advances in the line shape theory give validity and legitimacy to our measurement presented here. Optical oscillator strengths are derived from electron impact spectroscopy by analyzing the optical excitation as a function of momentum transfer, and taking the zero-momentum-transfer limit. This method is not as direct as the optical absorption method. Matthias *et al.* [12] measured the radiative lifetime of the $1s_4$ level using synchrotron radiation, and report a lifetime of 3.46(9) ns. This number appears inconsistent with the corresponding f value of 0.263(7) also listed in [12]. Many of the other higher accuracy measurements of the oscillator strength are in agreement with ours including the Hanle effect measurement by Anderson [9], the anomalous dispersion measurement by Smith *et al.* [15], the refractive index measurement by Bideau-Mehu *et al.* [16], and the electron impact measurement by Chan *et al.* [20]. The good agreement using these different methods is reassuring. The radiation trapping measurement by Weime and Mortier [10], Weime and Vanmarcke [14] and Salamero *et al.* [17] yielded lower f values for reasons discussed in the next section.

V. RADIATION TRAPPING SIMULATIONS

The experiments by Vermeersch *et al.* on resonance radiation trapping in Xe cover a pressure range from 2 mTorr to 10 Torr in a column of radius 1.8 cm at ambient temperature [2]. They used selective three-photon laser excitation of the $^3P_1^o$ resonance level. We compare in this section the results of our radiation trapping simulation using our refined oscillator strength to their experimental trapped decay rates.

The pressures studied by Vermeersch *et al.* cover the range of interest for lighting applications. Partial frequency redistribution (PFR) is important in this range. Vermeersch and Wieme [26] performed Monte Carlo simulations for comparison to the experimental work by Vermeersch *et al.* [2]. Their simulations were based on the Jefferies-White and Lee approximations for PFR [27–30]. They found that the experimental results were better, but not perfectly, reproduced by simulations based on the more realistic angle-dependent Lee operator. We confirm that the angle-dependent PFR operator yields simulated decay rates in better agreement with experimental decay rates.

Our version of the angle-dependent PFR operator for Monte Carlo simulations of radiation trapping has features that simplify and streamline the code. These features and the general structure of the code are described in the following paragraphs. They enabled us to completely avoid the use of numerical integration and of any "look-up" tables, both of which were used in the original Lee operator [28–30].

The initial radial coordinate ρ_i of the excited atom is chosen using a random number so that a desired production rate per unit volume or initial density of excited atoms is reproduced on the average. The position is recorded, and the frequency ν of the emitted photon is chosen from the Voigt profile. Let the reduced frequency x be

$$x \equiv \frac{\nu - \nu_0}{\nu_0 \sqrt{2k_B T/Mc^2}} , \tag{3}$$

where ν_0 is the line center frequency and M is the mass of the atom. Parker, Hitchon, and Lawler described an efficient random frequency generator for a Voigt profile [31]. Specifically, a normally distributed random number, x_{Doppler}, with a variance of one is chosen in the range of $-\infty$ to $+\infty$. We note that most computer software packages have a library function for generating normally distributed random numbers with a variance of one. This random number divided by $\sqrt{2}$ corresponds to a randomly chosen reduced frequency in a Doppler profile. Random numbers w_1 through w_7 uniformly distributed in the range 0 to 1 are chosen. The first of these is used to determine the frequency in the Lorentzian profile

TABLE I. Xenon 147-nm f values from the literature. The number in parentheses next to the f value is the uncertainty in the last digit(s).

Source	f-value	Method
	Experimental	
This work	0.264(16)	optical absorption
Anderson (1965)[a]	0.256(8)	Hanle effect
Chashchina & Schreider (1966)[b]	0.28(5)	optical absorption
Wilkinson (1966)[c]	0.26(2)	optical absorption
Geiger (1970)[d]	0.26(5)	electron impact spectroscopy
Wieme and Mortier (1973)[e]	0.214(20)	resonance radiation trapping
Delage and Carette (1976)[f]	0.183(73)	electron impact spectroscopy
Matthias *et al.* (1977)[g]	0.263(7)	radiative lifetime
Wieme and Vanmarcke (1979)[h]	0.226(25)	resonance radiation trapping
Smith *et al.* (1981)[i]	0.244(15)	anomalous dispersion
Bideau-Mehu *et al.* (1981)[j]	0.268(8)	refractive index
Salamero *et al.* (1984)[k]	0.226(26)	radiation trapping
Ferrell *et al.* (1987)[l]	0.260(50)	multiphoton ionization
Suzuki *et al.* (1991)[m]	0.222(27)	electron impact spectroscopy
Chan *et al.* (1992)[n]	0.273(14)	electron impact spectroscopy
	Theoretical	
Dow and Knox (1966)[o]	0.194	nonrelativistic Hartree-Fock
Gruzdev (1967)[p]	0.28	Coulomb approximation
Kim *et al.* (1968)[q]	0.212	nonrelativistic Hartree-Fock
Aymar *et al.* (1970)[r]	0.273	parametrized central potential
Geiger (1977)[d]	0.28	energy dependent quantum defect theory
Aymar and Coulombe (1978)[s]	0.282	parametrized central potential

[a]Reference 9.
[b]Reference 4.
[c]Reference 3.
[d]Reference 13.
[e]Reference 10.
[f]Reference 11.
[g]Reference 12.
[h]Reference 14.
[i]Reference 15.
[j]Reference 16.
[k]Reference 17.
[l]Reference 18.
[m]Reference 19.
[n]Reference 20.
[o]Reference 21.
[p]Reference 22.
[q]Reference 23.
[r]Reference 24.
[s]Reference 25.

$$w_1=\int_{-\infty}^{x_{\text{Lorentz}}}\frac{a_\nu}{\pi}\frac{1}{y^2+a_\nu^2}dy\ , \tag{4}$$

where a_ν is the Lorentz half width at half maximum divided by $\nu_0(2k_BT/M)^{1/2}/c$ and x_{Lorentz} is a reduced frequency. This analytic integral yields

$$x_{\text{Lorentz}}=a_\nu\tan[\pi(w_1-0.5)]\ . \tag{5}$$

The resultant frequency is given by

$$x_{\text{Voigt}}=x_{\text{Lorentz}}+\frac{x_{\text{Doppler}}}{\sqrt{2}}\ . \tag{6}$$

The distance the photon goes before being absorbed is given by

$$D=-\ln(w_2)\frac{\sqrt{2k_BT/M}}{N\pi r_e c f_{\text{lu}}\lambda L_V(x_{\text{Voigt}})}\ , \tag{7}$$

where $L_V(x_{\text{Voigt}})$ is the normalized Voigt profile, $\int L_V(y)dy=1$, which is evaluated using an analytic approximation based on a complex error function [31]. Emission of radiation is assumed to be isotropic, so the cosine of the polar angle is given by $\mu_i=2w_3-1$ and the azimuthal angle is given by $\phi_i=2\pi w_4$. We then find the new radial position of the resonance atom using

$$\rho_{i+1}=[\rho_i^2+D^2(1-\mu_i^2)+2D(1-\mu_i^2)^{1/2}\rho_i\cos\phi_i]^{1/2}\ . \tag{8}$$

Note that the $\phi=0$ axis is oriented along the direction of ρ_i. If the $i+1$ radius is outside the cylinder, the frequency and time taken (or number of steps) since the initial production of the photon are recorded. A new resonance atom is generated. If the photon did not escape, then the new position ρ_{i+1} of the resonance atom is recorded. The probability of a dephasing collision during a radiative lifetime is

$$P_c=\left[1+\frac{65.71g_l}{N\lambda^3 g_u}\right]^{-1}\ . \tag{9}$$

If w_5 is less than P_c the photon is reemitted using a random reduced frequency from a Voigt profile as described above. Otherwise the resonance atom did not have a dephasing collision and the frequency in the lab frame of the reemitted photon must be determined using appropriate Doppler shifts. The direction of the photon that excited the resonance atom at ρ_{i+1} is updated using

$$\phi_i'=\phi_i-\sin^{-1}\left[\frac{D(1-\mu_i^2)^{1/2}\sin\phi_i}{\rho_{i+1}}\right]\ . \tag{10}$$

This information is used in a Doppler shift calculation if no dephasing collision occurs.

The Doppler shift determination is one of the more intricate parts of the code. First, the axial velocity of the absorbing atom along the absorbed photon trajectory must be randomly selected from the distribution

$$p(u_a)=\frac{1}{L_V(x_{\text{Voigt}})}\left[\frac{a_\nu}{\pi^{3/2}}\frac{\exp(-u_a^2)}{a_\nu^2+(x_{\text{Voigt}}-u_a)^2}\right]\ , \tag{11}$$

where u_a is the reduced axial velocity [axial velocity divided by $(2k_BT/M)^{1/2}$], and where L_V is a normalized Voigt profile. The operator used to select a random u_a from this distribution depends on x_{Voigt}. Our code uses the same approximation used by Lee [29] for $|x_{\text{Voigt}}|>5$. The distribution for these large x_{Voigt} is approximated

$$p(u_a)\simeq\frac{1}{\pi^{1/2}}\exp\left[-\left[u_a-\frac{1.0}{x_{\text{Voigt}}}\right]^2\right] \tag{12}$$

and the normally distributed random number generator is called, the result is divided by $\sqrt{2}$, and then shifted by adding $1.0/x_{\text{Voigt}}$. Von Neumann's [32] method of rejection is used for $1.5\le|x_{\text{Voigt}}|\le5$. Our trial function for this range of $|x_{\text{Voigt}}|$ is different from that used by Lee in order to avoid numerical integration and look-up tables. We use a trial function $q(u_a)\ge p(u_a)$ where

$$q(u_a)=\begin{cases}-p(-1)u_a\exp(1.0-u_a^2) & \text{for } u_a<-1.0\\ \max[1.5p(0),p(|x_{\text{Voigt}}|-0.25)] & \text{for } -1\le u_a\le|x_{\text{Voigt}}|-0.25\\ p(|x_{\text{Voigt}}|-0.25)\dfrac{1+(0.25/a_\nu)^2}{1+\left[(u_a-|x_{\text{Voigt}}|)\dfrac{1}{a_\nu}\right]^2} & \text{for } |x_{\text{Voigt}}|-0.25<u_a\ .\end{cases} \tag{13}$$

Note that the indefinite integral

$$Q(u_a)=\int_{-\infty}^{u_a}q(y)dy \tag{14}$$

is analytic in each region. Furthermore, the function Q is easily inverted so that a trial u_a can be chosen using

$$u_a=Q^{-1}\{w_6Q(\infty)\}\ . \tag{15}$$

This u_a is accepted if

$$w_7<\frac{p(u_a)}{q(u_a)} \tag{16}$$

otherwise it is rejected and the two preceding steps are repeated. When a u_a is accepted, it is multiplied by the sign of x_{Voigt}. The trial function we use has a significant advantage over that used by Lee in that it avoids any numerical integration and any look-up tables [30]. Finally for $|x_{\text{Voigt}}|<1.5$ we follow Lee [30] and use the method of rejection with a trial function

$$q(u_a)=\frac{1}{\pi^{3/2}L_V(x_{\text{Voigt}})}\left[\frac{a_\nu}{a_\nu^2+(x_{\text{Voigt}}-u_a)^2}\right]\ . \tag{17}$$

Equations (14), (15), and (16) are used with this trial function.

After the axial velocity of the absorbing atom is determined, the normally distributed random number generator is used with appropriate $1/\sqrt{2}$ scaling to determine the transverse component u_t of the reduced velocity of the absorbing atom. The frequency of the photon is then Doppler shifted into the rest frame of the atom. The reemitted photon direction (μ_{i+1},ϕ_{i+1}) is chosen from an isotropic distribution and the frequency of the reemitted photon in the lab frame is computed using a Doppler shift from the rest frame of the atom, specifically

$$x_{i+1}=x_{\text{Voigt}}+u_a(\hat{\mathbf{n}}_{i+1}\cdot\hat{\mathbf{n}}_i'-1.0) +u_t\sqrt{1.0-(\hat{\mathbf{n}}_{i+1}\cdot\hat{\mathbf{n}}_i')^2}\ , \tag{18}$$

where $\hat{n}_i'$ is the unit vector in the direction of the photon prior to absorption, where $\hat{n}_{i+1}$ is the unit vector in the direction of the reemitted photon, and where

$$\hat{\mathbf{n}}_{i+1}\cdot\hat{\mathbf{n}}_i'=\mu_{i+1}\mu_i+\sqrt{1-\mu_{i+1}^2}\sqrt{1-\mu_i^2}\cos(\phi_{i+1}-\phi_i')\ . \tag{19}$$

The fundamental mode decay rates shown in Fig. 2 are determined using a spatially uniform initial density of resonance atoms by recording the "late time" escape rate (after many emission-absorption cycles). The second dip in the trapped decay rate near 3 Torr ($N\approx10^{17}$ cm^{-3}) is not due to PFR. Vermeersch *et al.* suggest that it is due to quasistatic resonance collisional broadening [2]. We see evidence for this effect in our experiment. The apparent f values deduced from our experimental equivalent widths greater than 10 cm^{-1} using Eq. (2) are smaller than 0.264. Both observations are consistent with the line profile more than 5 cm^{-1} from line center at pressures of 3–10 Torr decreasing more rapidly than a Lorentzian. This effect is not yet included in the radiation trapping simulations.

The second dip in the trapped decay rate as a function of pressure caused older determinations of the f value based on measurements of trapped decay rates to yield f values that were too small [10,14,17]. The quality of the experimental data by Vermeersch *et al.* [2] is sufficiently high to clearly reveal the second dip. The effect in older experiments of the unrecognized second dip was to reduce the trapped decay rate average for different pressures and thus reduce the measured f value.

The solid curve in Fig. 2 represents Monte Carlo results using our value $f_{\text{lu}}=0.264$, and the dotted curve represents Monte Carlo results using $f_{\text{lu}}=0.226$ [14]. At higher pressures (>0.1 Torr) the trapped decay rate scales in direct proportion to the vacuum decay rate and thus to the oscillator strength. Resonance collisional broadening (with complete frequency redistribution) dominates the radiation transport at higher pressures. The probability of a photon escaping in an absorption-emission cycle is independent of gas density in this high pressure regime. At lower pressures (<0.01 Torr) the trapped decay rate is less sensitive to the oscillator strength used in the simulation. The effect of a smaller oscillator strength at lower pressures is to decrease both the vacuum decay rate and the Doppler broadened absorption cross section. The decrease in the absorption cross section partially cancels the effect of a smaller vacuum decay rate in determining the trapped decay rate. The shape of the curve in Fig. 2 depends on the oscillator strength because the trapped decay rate depends on the oscillator strength in a nonlinear fashion.

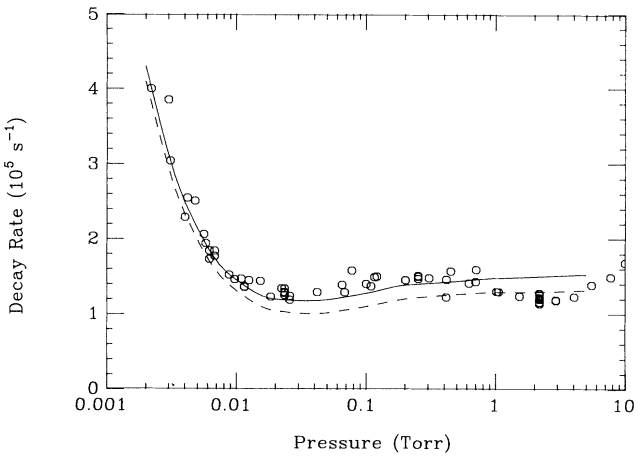

FIG. 2. Trapped decay rate for the xenon 147-nm transition as a function of pressure. Experimental points are from Ref. [2]. The solid line is from our Monte Carlo simulations using our result $f_{lu}=0.264$. The dashed line is from our Monte Carlo simulation using $f_{lu}=0.226$ [14].

VI. SUMMARY

A measurement, 0.264(16), for the absorption oscillator strength of the xenon 147-nm resonance transition is reported. This value is from direct absorption measurements with equivalent widths of ≈1 to ≈10 cm^{-1}. Equivalent widths in this range correspond to a part of the curve of growth which is well understood. The present oscillator strength measurement is compared to older values in the literature.

Monte Carlo simulations of resonance radiation trapping are run using the f value of 0.264 and using angle-dependent partial frequency redistribution. The simulated trapped decay rates are in good agreement over a wide range of gas density with the trapped decay rate measured by Vermeersch *et al.* [2].

ACKNOWLEDGMENTS

This research is supported by the General Electric Company and the National Institute of Standards and Technology under the Advanced Technology Program.

[1] D. A. Doughty, Bull. Am. Phys. Soc. **38**, 2356 (1993).
[2] F. Vermeersch, N. Schoon, E. Desoppere, and W. Wieme, in *Optogalvanic Spectroscopy,* edited by R. S. Stewart and J. E. Lawler, IOP Conf. Proc. No. 113 (Institute of Physics and Physical Society, London, 1991), p. 133.
[3] P. G. Wilkinson, J. Quant. Spectrosc. Radiat. Transfer **6**, 823 (1966).
[4] G. I. Chashchina and E. Ya. Shreider, Opt. Spectrosc. **20**, 283 (1966).
[5] H. Kopfermann and E. Rindal, Z. Phys. **87**, 460 (1934).
[6] D. A. Jackson, M. C. Coulombe, and J. Bauche, Proc. R. Soc. London, Ser. A **343**, 443 (1975).
[7] A. Corney, *Atomic and Laser Spectroscopy* (Clarendon, Oxford, 1977), p. 262.
[8] J. M. Bridges and W. R. Ott, Appl. Opt. **16**, 367 (1977).
[9] D. K. Anderson, Phys. Rev. **137**, A21 (1965).
[10] W. Wieme and P. Mortier, Physica **65**, 198 (1973).
[11] A. Delage and J. D. Carette, Phys. Rev. A **14**, 1345 (1976).
[12] E. Matthias, R. A. Rosenberg, E. D. Poliakoff, M. G. White, S. T. Lee, and D. A. Shirley, Chem. Phys. Lett. **52**, 239 (1977).
[13] J. Geiger, Phys. Lett. **33A**, 351 (1970); Z. Phys. A **282**, 129 (1977).
[14] W. Wieme and M. Vanmarcke, Phys. Lett. A **72**, 215 (1979).
[15] P. L. Smith, G. G. Lombardi, B. L. Cardon, and W. H. Parkinson, Appl. Optics **20**, 647 (1981).
[16] A. Bideau-Mehu, Y. Guern, R. Abjean, and A. Johannin-Gilles, J. Quant. Spectrosc. Radiat. Transfer **25**, 395 (1981).
[17] Y. Salamero, A. Birot, H. Brunet, J. Galy, and P. Millet, J. Chem. Phys. **80**, 4774 (1984).
[18] W. R. Ferrell, M. G. Payne, and W. R. Garrett, Phys. Rev. A **35**, 5020 (1987).
[19] T. Y. Suzuki, Y. Sakai, B. S. Min, T. Takayanagi, K. Wakiya, H. Suzuki, T. Inaba, and H. Takuma, Phys. Rev. A **43**, 5867 (1991).
[20] W. F. Chan, G. Cooper, X. Guo, G. R. Burton, and C. E. Brion, Phys. Rev. A **46**, 149 (1992).
[21] J. D. Dow and R. S. Knox, Phys. Rev. **152**, 50 (1966).
[22] P. F. Gruzdev, Opt. Spectrosc. **22**, 170 (1967).
[23] Y. Kim, M. Inokuti, G. E. Chamberlain, and S. R. Mielczarek, Phys. Rev. Lett. **21**, 1146 (1968).
[24] M. Aymar, S. Feneuille, and M. Klapisch, Nucl. Instrum. Methods **90**, 137 (1970).
[25] M. Aymar and M. Coulombe, At. Data Nucl. Data Tables **21**, 537 (1978).
[26] F. Vermeersch and W. Wieme, in *Optogalvanic Spectroscopy* (Ref. 2), p. 109.
[27] J. T. Jefferies and O. R. White, Astrophys. J. **132**, 767 (1960).
[28] J. S. Lee, Astrophys. J. **192**, 465 (1974).
[29] J. S. Lee, Astrophys. J. **218**, 857 (1977).
[30] J. S. Lee, Astrophys. J. **255**, 303 (1982).
[31] G. J. Parker, W. N. G. Hitchon, and J. E. Lawler, J. Phys. B **26**, 4643 (1993).
[32] J. von Neumann, NBS Appl. Math. Series **12**, 36 (1951).